The structural manipulation of a series of Ni4 defective dicubanes: Synthesis, X-ray Structures, Magnetic and Computational analyses

Dalton Transactions

An international journal of inorganic chemistry

Accepted Manuscript

This article can be cited before page numbers have been issued, to do this please use: S. Woodhouse, T. N. Dais, E. H. Payne, M. K. Singh, E. K. Brechin and P. Plieger, *Dalton Trans.*, 2021, DOI: 10.1039/D0DT04286B.

ROYAL SOCIETY OF CHEMISTRY

rsc.li/dalton

View Article Online
DOI: 10.1039/D0DT04286B

Journal Name

ARTICLE TYPE

Cite this: DOI: 00.0000/xxxxxxxxxx

The Structural Manipulation of a Series of Ni_4 Defective Dicubanes: Synthesis, X-ray Structures, Magnetic and Computational Analyses.†

Sidney S. Woodhouse,[a] Tyson N. Dais,[a] Emily H. Payne,[b] Mukesh K. Singh,[b] Euan K. Brechin,[b] and Paul G. Plieger*[a]

Received Date
Accepted Date

DOI: 00.0000/xxxxxxxxxx

We report the synthesis and characterization of four new tetranuclear Ni(II) complexes, **C1**-**C4**, all of which exhibit defective dicubane cores. **C1**-**C4** are derived from the same salicylaldoxime derived ligand, H_2**L1**. Complexes **C1** and **C4** have isostructural cores, differing in structure only by solvate molecules. Magnetic and computational analyses have revealed that complexes **C1**, **C2**, and **C4** exhibit competing ferro- and antiferromagnetic interactions, however the different solvated species in **C1** and **C4** leads to notably different magnitudes in their magnetic coupling constants. Theoretical magneto-structural studies show that the pairwise magnetic exchange interaction is highly dependent on the Ni–X–Ni angle, as revealed by orbital overlap calculations.

Introduction

The last few years have seen an increased interest in transition metal (3*d*) based polynuclear coordination complexes, due to continued interest in fields such as catalysis,[1–3] luminescence,[4] and single molecule magnetism.[5–9] A popular topology found in both of these fields is defective dicubanes, more commonly known as butterfly complexes.[9–11] Defective dicubane refers to tetranuclear complexes where two face-sharing cubanes, each missing an opposite vertex, form the metallic core (Fig. 1).[8,10,12–14] Defective dicubanes have gained popularity due to the coordination chemist's ability to manipulate exchange interactions through synthetic chemistry.[15–18] For example, tuning of exchange interactions has been shown to be an effective method for quenching quantum tunnelling of magnetization (QTM).[16,19,20] Common manipulation methods include changing the bridging groups between the metal ions, or introducing groups either coordinated or free that can form inter/intramolecular interactions, which change the bridging angles, and therefore change the sign and/or magnitude of magnetic interactions.[15,17,18,21] This is well reported in the literature, with examples by Oyarzabal *et al.*,[22] and Jiang *et al.*,[21] who show that by switching the central bridging group from a methoxo group to an azido group, a stronger ferromagnetic exchange between the two metal centres can be achieved.

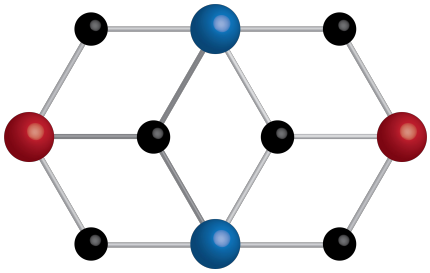

Fig. 1 Schematic representation of the defective dicubane topology, showing the "wingtip" positions in red, the "body" positions in blue, and the bridging atoms in black.

The salicylaldoxime moiety is commonly found in 3*d* based coordination clusters. The popularity surrounding salicylaldoxime derivatives as chelating ligands arises from the number of coordination sites (phenoxo oxygen and oximato nitrogen and oxygen) present, but more importantly, from its ability to impart structural torsion through M–N–O–M (M = metal ion) bridging (Fig. 2), often resulting in interesting magnetic properties.[23,24] This structural torsion is commonly seen in complexes with a triangular metallic core,[25] such as the Mn^{III} complex produced by Brechin and coworkers which exhibited single molecule magnetism, and at the time, was a record breaking single molecule magnet (SMM).[6] Although this structural torsion is more commonly seen in triangular topolo-

[a] *School of Fundamental Sciences, Massey University, Private Bag 11 222, Palmerston North, New Zealand; E-mail: p.g.plieger@massey.ac.nz*
[b] *EaStCHEM School of Chemistry, The University of Edinburgh, David Brewster Road, Edinburgh, EH93FJ, Scotland, United Kingdom*

† Electronic Supplementary Information (ESI) available: Computational details, crystal data and structural refinement details can be found in the supporting information. See DOI: 00.0000/00000000.

‡ Manuscript and synthetic efforts completed by SSW, crystallographic analysis completed by TND, magnetic analysis completed by EHP and EKD, computational analysis completed by MKS, and manuscript editing completed by EKB and PGP.

View Article Online
DOI: 10.1039/D0DT04286B

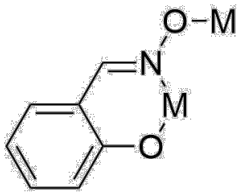

Fig. 2 Schematic representation of the classical M–N–O–M bridging found in salicylaldoxime derived coordination clusters.

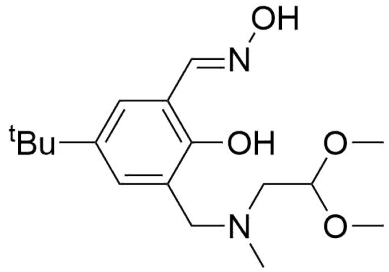

Fig. 3 Schematic of the ligand H_2**L1**, 5-*tert*-butyl-3-(*N*-methyl-*N*-(2,2-dimethoxyethyl)amino)methyl salicylaldoxime, utilized in this research.

gies, as previously mentioned, there are reported examples of this occurring in both cubes and defective dicubanes.[26–28] The $[Co^{II}_2Co^{III}_2(\mathbf{L})_2(H\mathbf{L})_2(N_3)_4(EtOH)_2]$ butterfly reported by Yao *et al.*[26] utilises the ligand 3-methoxysalicylaldoxime with the phenoxo oxygen and oximato group coordinating to the metal centres. The deprotonation of the oximato oxygen causes distortion within the metallic core, as the exchange coupling resembles the well known M–N–O–M oximato bridging rather than the more typical M–X–M (X = bridging group) bridging.

Our aim for this investigation was to synthesize and characterize, both magnetically and computationally, a series of Ni(II) defective dicubanes to explore how minor structural changes can affect the overall magnetic properties of a complex. The structural changes investigated involved changing the coordinated anions, and lattice solvent molecules. Four Ni(II) defective dicubanes have been synthesized, utilizing the salicylaldoxime derived ligand H_2**L1** (5-*tert*-butyl-3-(*N*-methyl-*N*-(2,2-dimethoxyethyl)amino)methyl salicylaldoxime, Fig. 3), $[Ni_4(H\mathbf{L1})_2(OMe)_2(OAc)_2Cl_2]\cdot(Et_2O)_3$ (**C1**), $[Ni_4(H\mathbf{L1})_2(OMe)_2(MeOH)_2Cl_4]\cdot Et_2O$ (**C2**), $[Ni_4(H\mathbf{L1})_2(OMe)_2(MeOH)_2Cl_{2.8}F_{1.2}]\cdot Et_2O$ (**C3**), and $[Ni_4(H\mathbf{L1})_2(OMe)_2(OAc)_2Cl_2]\cdot(MeOH)_2$ (**C4**). We report the synthesis, X-ray structures, magnetic, and computational analysis of complexes **C1**-**C4**.

Results and discussion

Structural Analysis

The solid-state complexes, **C1**-**C4**, have been synthesized from the reaction between H_2**L1** and Ni(II) metal salts ($Ni(OAc)_2\cdot 4H_2O$, $NiCl_2\cdot 6H_2O$, and $Ni(BF_4)_2\cdot 6H_2O$) in MeOH at room temperature (RT). Successful coordination between H_2**L1** and the Ni(II) ions was confirmed visually by the yellow ligand solution turning green. Isolation of complexes **C1**-**C4** was achieved by slow

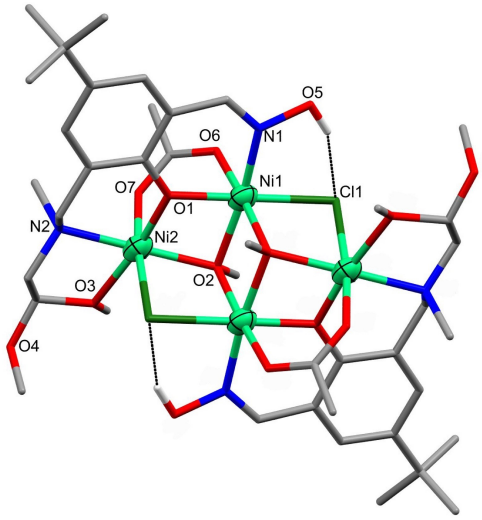

Fig. 4 Molecular structure common to complexes **C1** and **C4**. Lattice solvent molecules and non-interacting hydrogen atoms removed for clarity. Colour code: Ni = light green, N = blue, O = red, Cl = dark green, C = grey, and H = white. Hydrogen bonds represented as black dotted lines. Figs. of **C1** and **C4** with free solvent molecules can be found in the supporting material, Fig. S1.

vapour diffusion of Et_2O into the concentrated green methanolic solution.

All complexes are monoclinic, crystallizing in the $P2_1/c$ space group (Table S1). The general structure of **C1**-**C4** consists of a defective dicubane with four Ni(II) ions, each with distorted octahedral geometries (Tables 1 and S2) and donor sets consisting of oxygen, nitrogen, chloride, and fluoride atoms. For complexes **C1** and **C4**, the asymmetric unit contains half of the structure, with the remainder symmetry generated and for complexes **C2** and **C3**, the asymmetric unit contains the whole structure (the full structures of **C1**-**C4** can be seen in Figs. 4 - 6).

The metallic cores of the four Ni(II) defective dicubanes have similar coordination environments, with complexes **C1** and **C4** being isostructural. For all complexes, the central Ni(II) ions, nicknamed the "body" ions, have a coordination environment consisting of a terminal $N_{oximato}$ and bridging μ_2-$O_{phenoxo}$ from the ligand and three additional bridging groups: two μ_3-$O_{methoxo}$ and a μ_2-X_{halide} (μ_2-Cl for **C1**, **C2**, and **C4** and μ_2-Cl/μ_2-F in a 40:60 ratio for **C3**). The coordination environment of the Ni(II) ions is completed by either a μ_2-OAc (**C1** and **C4**) or a MeOH molecule (**C2** and **C3**). The outer Ni(II) ions, nicknamed the "wingtip" ions, have coordination environments consisting of terminal O_{OCH_3} and N_{amino} groups and a bridging μ_2-$O_{phenoxo}$, all from the ligand. The remainder of the coordination environment is made up of a μ_3-$O_{methoxo}$, a μ_2-X_{halide} (μ_2-Cl for **C1**, **C2**, and **C4** and μ_2-Cl/μ_2-F in a 40:60 ratio for **C3**) and either a μ_2-OAc (**C1** and **C4**) or a terminal chloride (**C2** and **C3**). For all complexes, hydrogen bonds can be found between the oximato OH group and the bridging μ_2-$X_{halide/s}$. Additional hydrogen bonds can be found for complexes **C2** and **C3** between the terminal chlorides and MeOH groups. For all complexes, solvent molecules are found within the crystal lattices. For complexes, **C1**-**C3**, Et_2O

View Article Online
DOI: 10.1039/D0DT04286B

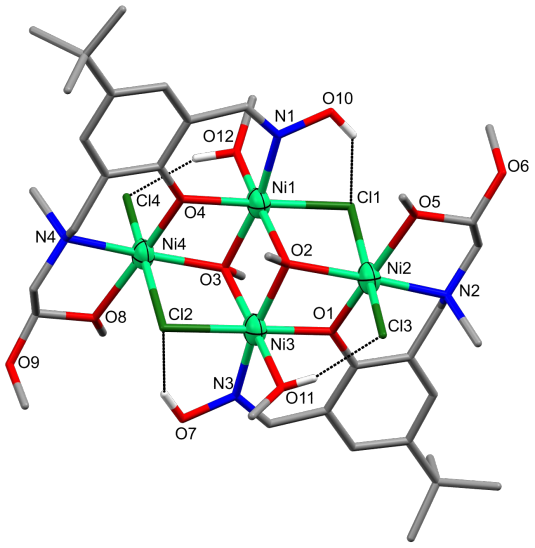

Fig. 5 Molecular structure of **C2**. Lattice solvent molecules and non-interacting hydrogen atoms removed for clarity. Colour code: Ni = light green, N = blue, O = red, Cl = dark green, C = grey, and H = white. Hydrogen bonds represented as black dotted lines.

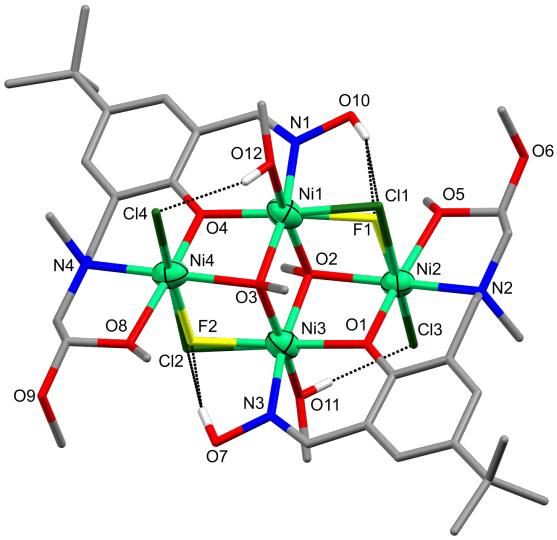

Fig. 6 Molecular structure of **C3**. Lattice solvent molecules and non-interacting hydrogen atoms removed for clarity. Colour code: Ni = light green, N = blue, O = red, Cl = dark green, F = yellow, C = grey, and H = white. Hydrogen bonds represented as black dotted lines.

molecules (one molecule for both **C2** and **C3**, and two molecules, with one positionally disordered over two sites for **C1**) are found in the crystal lattice. For complex **C4**, two MeOH solvates each form a hydrogen bond with an oxygen atom of the bridging acetate groups.

The main structural difference between complexes **C1** and **C4** are the solvate molecules in the lattice (Et_2O and MeOH respectively). The additional hydrogen bonding between the methanol solvate and the metallic core of **C4** results in different crystal packing, with the intramolecular Ni1–Ni1' distances of **C1** and **C4** being 13.86 Å and 10.91 Å within the same crystal plane respectively, and 9.94 Å and 10.15 Å between different crystal planes respectively (Figs. S2 and S3), but more importantly, results in small changes to the Ni–X–Ni angles of the exchange pathways in **C1** and **C4** (Tables 1 and S3) resulting in significant difference in the magnetic properties.

For complex **C3**, the presence of bridging fluoride anions has resulted in a large amount of disorder, with the μ_2-halide bridges being both fluoride and chloride (60:40 respectively). The initial goal for this structure was to retain the bridging chloride groups while incorporating fluoride caps, as a mixed-halide analogue to complex **C2**. This small difference between complexes **C2** and **C3**, has resulted in large changes in the magnetic properties.

Magnetic Analysis

The direct-current molar magnetic susceptibilities, χ_M, of polycrystalline samples of complexes **C1**-**C4** were measured in an applied magnetic field, B = 0.1 T, over the 290 - 2 K temperature range. The experimental results are shown in Fig. 7 as the $\chi_M T$ product versus T. At 300 K, the $\chi_M T$ products (5.12 (**C1**), 5.25 (**C2**), 4.91 (**C3**), 5.48 (**C4**) cm^3Kmol^{-1}) are consistent with the expected value for four uncorrelated Ni(II) ions (S_{Ni} = 1; 5.06 cm^3Kmol^{-1}) with g_{Ni} = 2.25. Upon cooling, the $\chi_M T$ products of **C1**, **C2** and **C4** rise slowly reaching maximum values of 5.82 (T = 22 K), 5.62 (T = 18 K) and 10.72 (T = 3.7 K) cm^3Kmol^{-1}, respectively. Upon further cooling, the $\chi_M T$ products fall to 4.43 (**C1**), 4.42 (**C2**) and 9.87 (**C3**) cm^3Kmol^{-1} at 2 K. Given that the expected $\chi_M T$ value for a ferromagnetically coupled [Ni^{II}_4] unit (S = 4) is 12.66 cm^3Kmol^{-1} the experimental susceptibility data is likely due to competing ferro- and antiferromagnetic exchange interactions, in tandem with zero-field splitting effects and/or antiferromagnetic intermolecular interactions at the lowest temperatures. For **C3**, the $\chi_M T$ product remains constant with decreasing temperature until ~77 K, at which point it falls sharply to a minimum value of 1.58 cm^3Kmol^{-1} at 2 K. This is indicative of the presence of dominant antiferromagnetic exchange.

To better define the low-temperature magnetic properties, variable-temperature-variable-field (VTVB) magnetization measurements were performed in the temperature and field ranges of 3 - 6 K and 0.5 - 7 T (Fig. 8). The magnetization reaches a maxima (3 K, 7 T) of 7.59 (**C1**), 7.02 (**C2**), 7.02 (**C3**), and 8.77 (**C4**) μ_B. The susceptibility and magnetization data of **C1**, **C2**, and **C4** were fitted simultaneously using the program PHI[29] with the following spin-Hamiltonian (1):

where the summation indices *i,j* label consecutive metal cen-

View Article Online
DOI: 10.1039/D0DT04286B

Table 1 Averaged bond lengths (Å) and bond angles (°) of complexes **C1**-**C4**

	C1	**C2***	**C3***	**C4**
Ni1-Cl1	2.50(8)	2.40	2.29	2.42(1)
Ni1-O1	2.04(19)	2.00	2.01	2.00(3)
Ni1-O2	2.01(19)	2.07	2.06	2.05(3)
Ni1-O6	2.11(2)	—	—	2.07(3)
Ni1-O11	—	2.08	2.10	—
Ni1-N1	1.98(2)	2.05	2.01	2.05 (3)
Ni1-O2	2.12(19)[a]	2.08	2.05	2.07(3)[b]
Ni1-F1	—	—	2.10	—
Ni2-O1	1.95(19)[a]	2.02	2.03	2.00(3)[b]
Ni2-O2	2.08(19)	2.08	2.09	2.06(3)
Ni2-O7	2.07(2)	—	—	2.02(3)
Ni2-O3/5	2.09(2)	2.17	2.17	2.16(3)
Ni2-N2	2.12(2)	2.09	2.08	2.09(4)
Ni2-Cl1	2.56(8)	2.47	2.48	2.47(1)
Ni2-Cl3	—	2.37	2.36	—
Ni2-F1	—	—	2.04	—
Ni1-O2-Ni1/3	98.8(8)[a]	95.64	94.96	98.24(11)[b]
Ni1-O1-Ni2/4	95.4(8)[a]	100.35	99.64	94.76(12)[b]
Ni1-Cl1-Ni2	86.3(2)	86.79	84.82	85.60(3)
Ni1-F1-Ni2	—	—	102.09	—
Ni1-O2-Ni2	92.1(8)	106.91	102.25	108.08(18)
Ni2-O2-Ni1/3	111.3(8)[a]	96.81	96.03	91.22(14)[b]

* Averaged values, non-averaged values found in Table S2
[a] 1-X, -Y, 1-Z
[b] 1-X, 1-Y, 1-Z

View Article Online
DOI: 10.1039/D0DT04286B

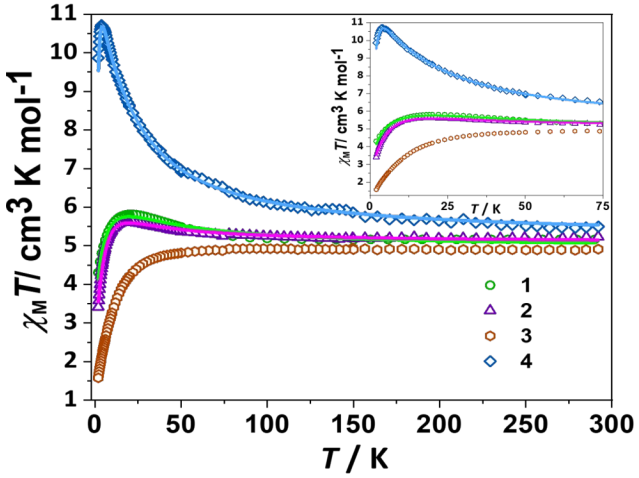

Fig. 7 $\chi_M T$ vs T for **C1**-**C4** in the range T = 2 - 290 K in a field, B = 0.1 T. The solid green (**C1**), purple (**C2**) and blue (**C4**) lines are the corresponding fit of the experimental data, as described in the text. The inset shows the same data in the 2 - 75 K range.

$$\hat{H} = \sum_i D_i(\hat{S}_{z,i}^2 - \frac{1}{3}S_i(S_i+1)) + \mu_B B\sum_i g_i\hat{S}_i - 2\sum_{i,j<1} J_{i,j}\hat{S}_i\cdot\hat{S}_j \quad (1)$$

tres, D is the uniaxial single-ion anisotropy parameter of Ni(II), $\hat{S}$ is a spin operator, S is the total spin, and J is the isotropic exchange interaction parameter. A model was employed using three different exchange pathways representing the wing-body (J_1 (Ni-O_2-Ni), J_2 (Ni-O/Cl-Ni)) and body-body (J_3 (Ni-O_3-Ni)) interactions typical for a [M_4] butterfly and which reflect the significantly different Ni-X-Ni angles present. The exchange pathways are schematically represented in Fig. 9, with the fitted values given in Table 2. The calculated values of the exchange and single ion anisotropy are consistent with those in the literature for octahedral Ni(II) ions in similar coordination spheres.[30–33] The data for **C3** were not fitted since the disordered chloride/fluoride bridges result in very different structural parameters (Table S3).

Computational Analysis

In order to estimate the exchange coupling values (J_1, J_2, and J_3) we have performed DFT calculations on the full X-ray structures of complexes **C1**-**C4**. Pairwise exchange interaction calculations were performed by keeping only two paramagnetic Ni(II) centres, replacing the remaining two with Zn(II). See Computational Details section for more information. For μ_2-Cl/F moieties, we consider only the F-bridged structure, since the Cl-bridged structure is analogous to compound **C2**. The DFT calculated J values (Table 3) are in excellent agreement with the experimental values (Table 2). The J_1 exchange interaction, which is mediated via μ_3-$O_{methoxo}$, μ_2-$O_{phenoxo}$, and μ_2-OAc groups for **C1** and **C4**, with average Ni-$\mu_{2/3}$O-Ni angles of 93.7/93.0°, respectively (Table S4), is estimated to be moderately ferromagnetic (+9.7 cm^{-1} (**C1**), +9.2 cm^{-1} (**C4**)). Overlap calculations suggest one moderate overlap for both **C1** and **C4** ($\langle Ni(1)d_{z^2}|p_{x/y/z}|Ni(2)d_{z^2}\rangle = 0.041$ for both **C1** and **C4**, Table S5; Fig. S4) and three small/orthogonal magnetic orbital overlaps resulting in ferromagnetic exchange. Previous studies on polymetallic Ni(II) complexes highlight the importance of the Ni-$\mu_{2/3}$O-Ni angle on the magnetic exchange coupling value: the larger the angle the larger the antiferromagnetic contribution, the crossover between ferro- and antiferromagnetic being ~97-98°.[34–37] In addition to this, it has been shown previously that the presence of a bridging phenoxo group in tandem with a bridging carboxylate group exhibits a counter-complementary effect, often resulting in a ferromagnetic interaction.[38] The J_1 magnetic exchange interaction for complexes **C2** and **C3**, mediated by μ_3-$O_{methoxo}$ and μ_2-$O_{phenoxo}$ bridging groups with average Ni-$\mu_{2/3}$O-Ni angles of 98.6°and 97.8°, respectively (Table S4), shows weak antiferromagnetic exchange (-2.3 cm^{-1} (**C2**) and -0.3 cm^{-1} (**C3**)). One strong ($\langle Ni(1)d_{z^2}|p_{x/y/z}|Ni(2)d_{x^2-y^2}\rangle = 0.061$ (**C2**) and $\langle Ni(1)d_{x^2-y^2}|p_{x/y/z}|Ni(2)d_{x^2-y^2}\rangle = 0.050$ (**C3**), Table S5) and three small/orthogonal magnetic orbital overlaps result in weak antiferromagnetic exchange.

The J_2 exchange interaction is mediated by μ_3-$O_{methoxo}$ and μ_2-Cl/F groups with average Ni–$\mu_{2/3}$(O/Cl/F)–Ni angles of 98.8°(**C1**), 96.8°(**C2**), 102.4°(**C3**), and 96.7°(**C4**) (Table S4), resulting in weak antiferromagnetic interactions in **C1** and **C4** (-1.5 cm^{-1} and -0.8 cm^{-1}, respectively), a moderate antiferromagnetic interaction in complex **C3** (-7.7 cm^{-1}) and a weak ferromagnetic interaction for complex **C2** (+2.1 cm^{-1}). Overlap calculations suggest two moderate overlap interactions for **C1** ($\langle Ni(2)d_{x^2-y^2}|p_{x/y/z}|Ni(3)d_{z^2}\rangle = 0.034$ and $\langle Ni(2)d_{x^2-y^2}|p_{x/y/z}|Ni(3)d_{x^2-y^2}\rangle = 0.036$, Table S5) and one strong interaction for **C4** ($\langle Ni(2)d_{x^2-y^2}|p_{x/y/z}|Ni3)(d_{x^2-y^2}\rangle = 0.055$, Table S5), leading to a small antiferromagnetic interaction. For **C3**, one strong and one moderate magnetic orbital overlap ($\langle Ni(2)d_{x^2-y^2}|p_{x/y/z}|Ni(3)d_{z^2}\rangle = 0.061$ and $\langle Ni(2)d_{z^2}|p_{x/y/z}|Ni(3)d_{z^2}\rangle = 0.036$, Table S5) results in a moderate antiferromagnetic interaction. For **C2**, only one moderate interaction ($\langle Ni(2)d_{x^2-y^2}|p_{x/y/z}|Ni(3)d_{x^2-y^2}\rangle = 0.035$, Table S5) is observed resulting in a small ferromagnetic interaction between the Ni(II) centres. Note that **C3** contains the more electronegative F-bridging group with a smaller average Ni–F distance resulting in a much stronger antiferromagnetic interaction compared to the Cl analogue. Although the average structural parameters for **C2** and **C4** are similar, there is a significant difference in sign and magnitude of the magnetic coupling (+2.1 cm^{-1} and -0.8 cm^{-1}, respectively). The Ni–μ_2Cl–Ni angle is 86.7°(**C2**) and 85.6°(**C4**) whereas the Ni–μ_3O–Ni angle is 107.0°(**C2**) and 107.8°(**C4**). In agreement with previously published magneto-structural studies,[34] the change in Ni–O–Ni angle gives a more dominant shift to antiferromagnetic coupling, compared to the small increased ferromagnetic contribution due to narrowing of the Ni–Cl–Ni angle, as supported by overlap calculations.

The J_3 exchange interaction for complexes **C1**-**C4** is mediated by two μ_3-$O_{methoxo}$ groups with average Ni–μ_3O–Ni angles of 98.9°, 95.7°, 95.0°, and 98.2°, respectively. This results in weak ferromagnetic exchange in complexes **C1** (+1.7 cm^{-1}) and **C4**

View Article Online
DOI: 10.1039/D0DT04286B

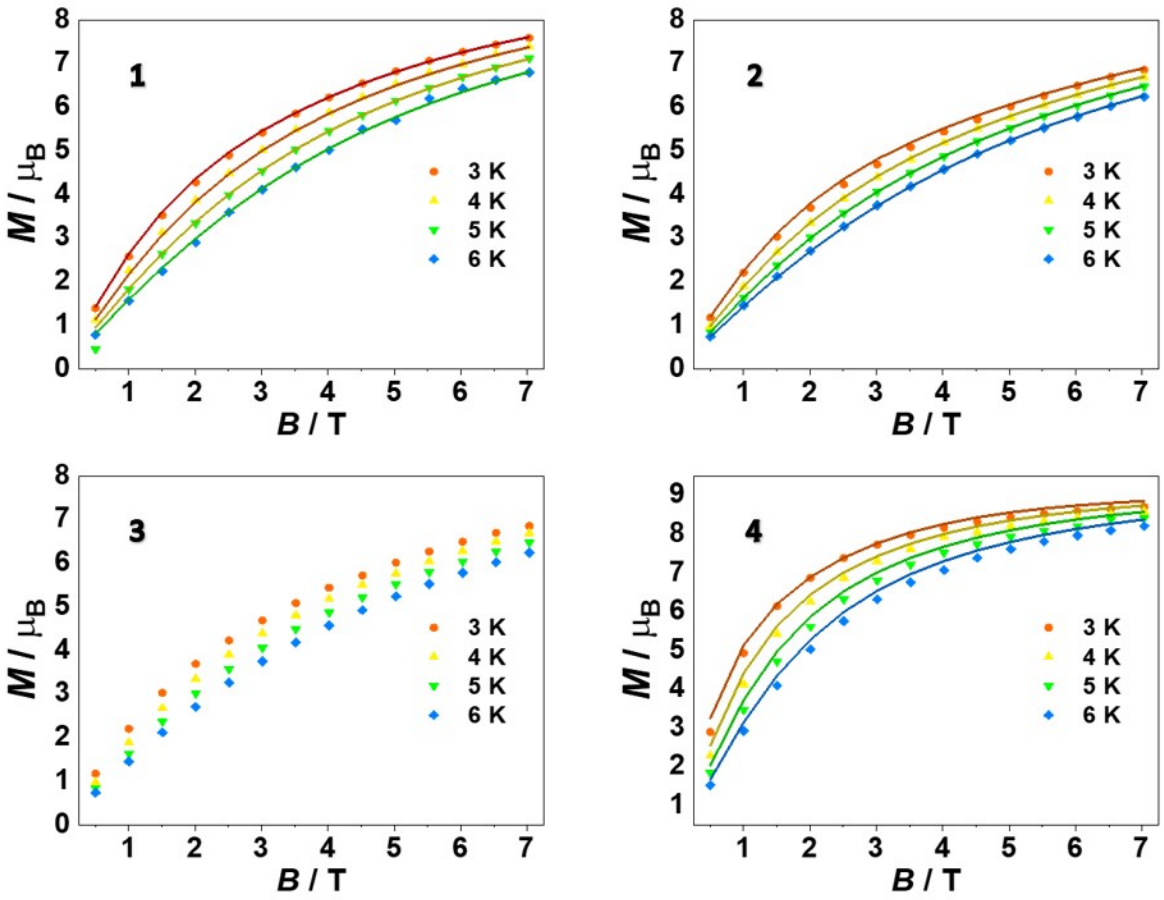

Fig. 8 Field dependence of the magnetization (M) measured in the T = 3 - 6 K and B = 0.1 - 7.0 T temperature and field ranges for **C1**, **C2**, **C3**, and **C4**. The solid lines are a fit of the experimental data. See main text for details.

Table 2 Fitted experimental magnetic exchange (J_1, J_2, and J_3) and anisotropy parameters (g and D_{Ni}) for **C1**, **C2**, and **C4**.

	J_1(cm^{-1})	J_2(cm^{-1})	J_3(cm^{-1})	g	D_{Ni}(cm^{-1})
C1	+1.92(±0.08)	-1.77(±0.07)	+8.19(±0.26)	2.22 (±0.002)	-9.3 (±0.07)
C2	-0.27(±0.02)	-0.17(±0.02)	+4.73(±0.07)	2.25(±0.001)	-15.1(±0.09)
C4	+7.94(±0.13)	-1.31(±0.12)	+6.67(±0.48)	2.28(±0.002)	-3.99(±0.07)

View Article Online
DOI: 10.1039/D0DT04286B

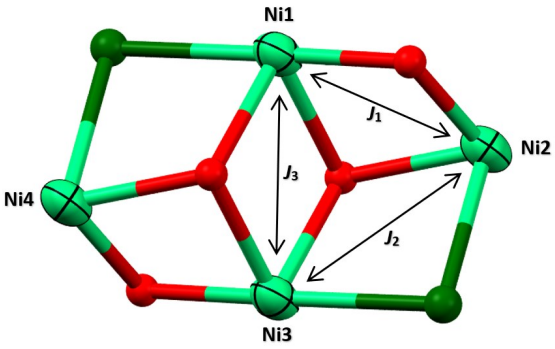

Fig. 9 The magnetic core common to compounds **C1**, **C2**, and **C4**, with the three different exchange interactions, J_1, J_2, and J_3. Colour code: Ni = light green, O = red, Cl = dark green.

Table 3 DFT computed magnetic exchange interactions for **C1**-**C4**. The values in bold are those obtained by performing calculations on dimeric models and the non-bold values were obtained by performing calculations on the full molecules. See the computational details section for more information.

	J_1(cm^{-1})	J_2(cm^{-1})	J_3(cm^{-1})
C1	+9.3/**+9.7**	-1.6/**-1.5**	+1.6/**+1.7**
C2	-2.9/**-2.3**	+1.8/**+2.1**	+9.1/**+9.7**
C3	-2.2/**-0.3**	-5.9/**-7.7**	+7.2/**+10.7**
C4	+9.7/**+9.2**	-0.3/**-0.8**	+0.3/**+1.3**

(+1.3 cm^{-1}) and moderate ferromagnetic exchange for complexes **C2** (+9.7 cm^{-1}) and **C3** (+10.7 cm^{-1}). Overlap calculations suggest the presence of one moderate overlap interaction for **C1** and **C4** ($\langle \mathrm{Ni}(1)d_{x^2-y^2}|p_{x/y/z}|\mathrm{Ni}(3)d_{x^2-y^2}\rangle = 0.043$ and 0.044 respectively, Table S5), which leads to a small ferromagnetic interaction. For **C2** and **C3**, none of the magnetic orbitals are interacting (Table S5), affording a relatively large ferromagnetic exchange interaction.

The spin density plots for **C1**-**C4** (Fig. 10, Fig. S5) suggest a spin delocalization mechanism with the spin density on the Ni(II) ions in the range 1.661 - 1.717. This is as expected since the unpaired electrons reside in the e_g orbitals.[39,40] Of all the bridging atoms, the largest spin density is detected on the μ_3-$O_{methoxo}$ atoms (0.162-0.168). The spin density on the μ_2-Cl bridging atoms (0.097-0.112) is greater than that on the μ_2-F bridging atoms (0.068-0.074), since the 3p orbitals of Cl are energetically closer to the 3*d* orbitals of the Ni(II) ions.

Conclusions

The reaction between ligand, H_2**L1**, and Ni(II) metal salts, $Ni(OAc)_2\cdot 4H_2O$, $NiCl_2\cdot 6H_2O$, and $Ni(BF_4)_2\cdot 6H_2O$, has resulted in the formation of four new tetranuclear Ni(II) defective dicubanes ($[Ni_4(HL1)_2(OMe)_2(OAc)_2Cl_2]\cdot(Et_2O)_3$ (**C1**), $[Ni_4(HL1)_2(OMe)_2(MeOH)_2Cl_4]\cdot Et_2O$ (**C2**), $[Ni_4(HL1)_2(OMe)_2(MeOH)_2Cl_{2.8}F_{1.2}]\cdot Et_2O$ (**C3**), and $[Ni_4(HL1)_2(OMe)_2(OAc)_2Cl_2]\cdot(MeOH)_2$ (**C4**)). The Ni(II) ions are bridged by a series of phenoxo, methoxo, chloride, and fluoride atoms originating from the Ni(II) metal salt used. Despite the similarities in the formulae and general structural topology of **C1**-**C4** there are significant geometric differences that result in rather different magnetic properties. Perhaps the most striking example comes from a comparison of isomorphous **C1** and **C4**. Here different solvation leads to different packing in the extended structure which in turn leads to different intramolecular Ni–X–Ni angles and thus different magnetic exchange interactions. This study highlights the subtle intricacies involved in controlling intramolecular geometries and hence the sign and magnitude of magnetic coupling constants, particularly those relating to non-coordinating species such as anions/cations and solvent of crystallization.

Experimental Section

General Details

All reactions were performed under aerobic conditions using chemicals and solvents as received, unless otherwise stated. The ligand starting materials, 5-*tert*-butylsalicylaldehyde[41] and 3-(bromomethyl)-5-*tert*-butylsalicylaldehyde[42] were prepared as described in the literature. ^{1}H and ^{13}C NMR spectra were recorded on a Bruker Avance 500 MHz spectrometer and reported relative to residual solvent. Mass spectra were obtained using a Dionex UltiMate 3000 spectrometer. IR spectra were recorded on a Nicolet 5700 FT-IR spectrometer using an ATR sampling accessory. UV/Vis spectra were collected using a Shimadzu UV-3101PC spectrophotometer. Elemental analyses were determined by the Campbell Microanalytical Laboratory at the University of Otago. Variable temperature, solid-state DC magnetic susceptibility data down to 2 K was performed on polycrystalline samples embedded in eicosane and was collected on a Quantum Design MPMS XL-5 SQUID magnetometer equipped with a 7 T DC magnet at The University of Edinburgh. Diamagnetic corrections were applied to the observed paramagnetic susceptibilities using Pascal's constants. All crystalline samples originated from single bulk complexation reactions, which were analysed by unit cell checks, IR spectroscopy, and elemental analysis.

X-ray Crystallography

The X-ray data for complexes **C1**-**C4** (Table S1) was collected at low temperature (K) on a Rigaku Spider diffractometer equipped with a copper rotating anode X-ray source, using graphite monochromated Cu Kα (λ = 1.54187 Å) X-rays, and a curved image plate detector. Crystals were mounted on MiTeGen loops using Fomblin(R) Y oil. Crystal Clear[43] was utilised for data collection and FS PROCESS in PROCESS-AUTO[44] for cell refinement and data reduction. Solution and refinement was achieved using Olex2,[45] and the structures were solved by Superflip[46–48] and refined using SHELXL[49] in Olex2.[45] Non-hydrogen atoms were refined anisotropically, hydrogen atoms were placed in calculated positions, and refined by using a riding model with fixed isotropic U_{iso} values.

View Article Online
DOI: 10.1039/D0DT04286B

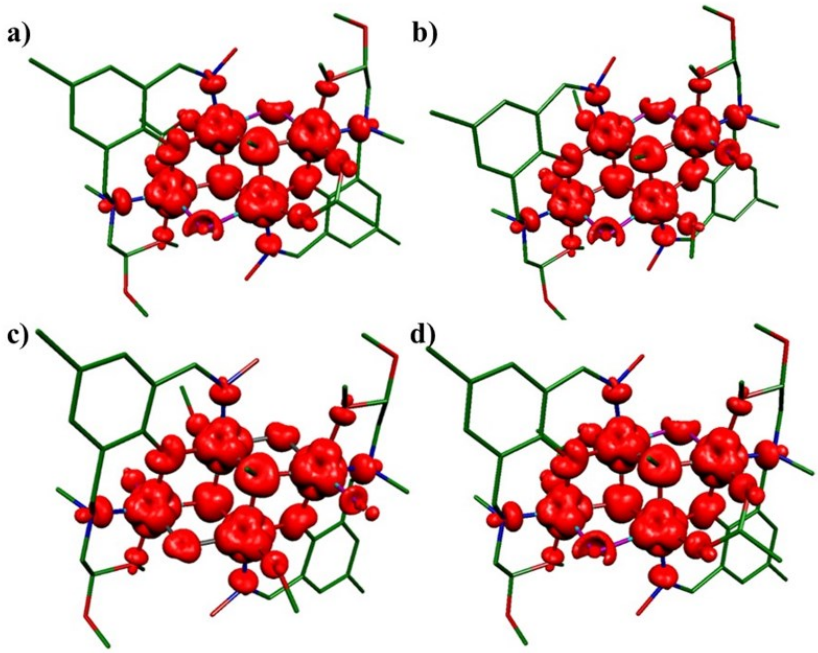

Fig. 10 Spin density plots for the high spin states of (a) **C1**, (b) **C2**, (c) **C3**, and (d) **C4**. Hydrogen atoms have been removed for clarity. The iso-density surface shown corresponds to a value of 0.005 e^-/bohr^3.

$$\begin{aligned}\hat{H} = &-2J_1(\hat{S}_{Ni1}\cdot\hat{S}_{Ni2}+\hat{S}_{Ni3}\cdot\hat{S}_{Ni4})\\ &-2J_2(\hat{S}_{Ni1}\cdot\hat{S}_{Ni4}+\hat{S}_{Ni2}\cdot\hat{S}_{Ni3})\\ &-2J_3(\hat{S}_{Ni1}\cdot\hat{S}_{Ni3})\end{aligned} \quad (2)$$

Computational Details

The Gaussian 16 program suite[50] was used to estimate the magnetic exchange coupling constants present in complexes **C1**-**C4**, employing the hybrid B3LYP functional[51–54] along with the TZV basis set[55–57] for Ni, Zn, Cl, F, O, N atoms and the 6-31G* basis set[58] for the C and H atoms. Density Functional Theory together with the broken symmetry approach[59–62] is known to be a reliable tool for estimating magnetic exchange interactions with a high level of accuracy. Eight spin configurations were used to calculate three possible exchange coupling constants. The computed spin configurations comprise a high spin configuration with all spins up (S = 4), four other spin configurations with one of the spin centres down (S = 2) and three remaining spin configurations with two spin centres down (S = 0). See Table S6 for full details. Pairwise exchange interaction calculations were performed by keeping only two paramagnetic centres, replacing the remaining two with Zn(II). We have performed overlap integral calculations[63] between non-orthogonal singly occupied molecular orbitals of the Ni(II) ions to analyse the sign and magnitude of magnetic exchange parameters for **C1**-**C4** using the Heisenberg-Dirac-Van Vleck Hamiltonian[64] (2).

Ligand and Complex Syntheses

5-*tert*-Butyl-3-(*N*-methyl-*N*-(2,2-dimethoxyethyl)amino)methyl salicylaldehyde (HL1a). Solutions of 2,2-dimethoxy-*N*-methylethanamine (0.47 mL, 3.71 mmol) and 3-(bromomethyl)-5-*tert*-butylsalicylaldehyde (1.03 g, 3.71 mmol), each in $CHCl_3$ (20 mL) were simultaneously added dropwise to a stirred solution of Et_3N (0.51 mL, 3.71 mmol) in $CHCl_3$ (20 mL). The resulting bright yellow solution was stirred at RT for 24 hours. The solution was washed with deionised H_2O (3 x 60 mL), and the combined organic layers were dried over anhydrous $MgSO_4$, filtered and concentrated *in vacuo* to afford a yellow oil (1.10 g, 97%). ^{1}H NMR (500 MHz, $CDCl_3$): δ 10.33 (s, 1H, C*H*=O), 7.62 (d, J = 2.2 Hz, 1H, Ar-*H*(σ-amine)), 7.35 (d, J = 2.2 Hz, 1H, Ar-*H*(σ-oxime)), 4.59 (t, J = 5.4 Hz, 1H, CH_2-C*H*), 3.77 (s, 2H, Ar-CH_2-N), 3.38 (s, 6H, O-CH_3), 2.66 (d, J = 5.4 Hz, 2H, N-CH_2-CH), 2.37 (s, 3H, N-CH_3), 1.30 (s, 9H, ^{t}*Bu*); ^{13}C NMR (125.7 MHz, $CDCl_3$): δ 192.4, 159.2, 141.9, 133.3, 125.0, 123.7, 122.0, 102.2, 59.6, 58.2, 53.7, 42.6, 34.1, 31.3; IR: $\bar{\nu}$ = 2957 (C-H), 1678 (C=O), 1652 (C-H), 1604 (C=C), 1395 (C-H), 1364 (O-H), 1124 (C-N), 1073 (C-O) cm^{-1}; MS: *m/z* (ESI) 310 $[M+H]^+$; UV/Vis (ε, L/mol cm) in MeOH: 337.0 (3286), 259.5 (7360), 218.0 (14258); elemental analysis calcd (%) for $C_{17}H_{27}NO_4$: C 65.99, H 8.80, N 4.53; found: C 66.55, H 8.64, N 4.76.

5-*tert*-Butyl-3-(*N*-methyl-*N*-(2,2-dimethoxyethyl)amino)methyl salicylaldoxime (H_2L1). A solution of $NH_2OH\cdot HCl$ (0.24 g, 3.53 mmol) in EtOH (30 mL) was neutralised with a solution of KOH (0.20 g, 3.53 mmol) in EtOH (30 mL). The filtered solution was added dropwise to a solution of H**L1a** (0.98 g, 3.53 mmol) in EtOH (50 mL). The resulting solution was stirred for 24 hours at RT. The light yellow

View Article Online
DOI: 10.1039/D0DT04286B

solution was concentrated *in vacuo* affording an oil, which was redissolved in $CHCl_3$ (30 mL). This solution was washed with deionised H_2O (3 x 30 mL) and the combined organic layers were dried over anhydrous $MgSO_4$, filtered and concentrated *in vacuo* affording H_2**L1** as a yellow oil (0.94 g, 91%). ^{1}H NMR (500 MHz, $CDCl_3$): δ 8.37 (s, 1H, C*H*=N), 7.36 (d, J = 2.5 Hz, 1H, Ar-*H*(σ-amine)), 7.13 (d, J = 2.5 Hz, 1H, Ar-*H*(σ-oxime)), 4.62 (t, J = 5.2 Hz, 1H, CH_2-C*H*), 3.74 (s, 2H, Ar-CH_2-N), 3.36 (s, 6H, O-CH_3), 2.67 (d, J = 5.2 Hz, 2H, N-CH_2-CH), 2.36 (s, 3H, N-CH_3), 1.27 (s, 9H, ^{t}*Bu*); ^{13}C NMR (125.7 MHz, $CDCl_3$): δ 154.2, 148.6, 141.6, 128.2, 123.6, 122.4, 117.7, 102.2, 60.2, 58.2, 53.6, 42.5, 34.0, 31.4; IR: $\bar{\nu}$ = 3279 (O-H), 2959 (C-H), 1616 (C=N), 1394 (C-H), 1363 (O-H), 1126 (C-N), 1070 (C-O) cm^{-1}; MS: *m/z* (ESI) 325 $[M+H]^+$; UV/Vis (ε, L/mol cm) in MeOH: 315.0 (3693), 261.0 (8515), 217.5 (18479).

$[Ni_4(HL1)_2(OMe)_2(OAc)_2Cl_2]\cdot(Et_2O)_3$ (C1). To a solution of H_2**L1** (0.421 g, 1.06 mmol) in MeOH (10 mL) was added solutions of $Ni(OAc)_2\cdot 4H_2O$ (0.526 g, 2.11 mmol) and NH_4Cl (0.0565 g, 1.06 mmol), both in MeOH (10 mL). The bright green solution was stirred at RT for 30 minutes. Isolation of the complex was achieved by the diffusion of Et_2O into the reaction solution. Green prism shaped X-ray quality crystals were produced after a period of eight weeks. The crystals were crushed and air dried prior to further analysis. Yield (0.169 g, 12%); IR: $\bar{\nu}$ = 3249 (O-H), 2953 (C-H), 1575 (C=N), 1486 (C=C), 1463 (C-H), 1414 (N-O), 1219 (C-O), 1030 (C-N) cm^{-1}; elemental analysis calcd (%) for $C_{40}H_{66}N_4O_{14}Cl_2Ni_4\cdot Et_2O\cdot 3H_2O$: C 41.92, H 6.56, N 4.44; found: C 42.07, H 6.24, N 4.51.

$[Ni_4(HL1)_2(OMe)_2(MeOH)_2Cl_4]\cdot Et_2O$ (C2). To a solution of H_2**L1** (0.0530 g, 0.163 mmol) in MeOH (10 mL) was added a solution of $NiCl_2\cdot 6H_2O$ (0.0775 g, 0.326 mmol) in MeOH (20 mL). The green solution was stirred at RT for 10 minutes, followed by the addition of Et_3N (0.140 mL, 0.979 mmol). The solution was stirred for a furrther 10 minutes at RT. Isolation of the complex was achieved by the diffusion of Et_2O into the reaction solution. Green platelet shaped X-ray quality crystals were produced after a period of three weeks. The crystals were crushed and air dried prior to further analysis. Yield (0.030 g, 15%); IR: $\bar{\nu}$ = 3291 (O-H), 2966 (C-H), 1560 (C=N), 1479 (C=C), 1462 (C-H), 1221 (C-O), 1128 (C-O), 1024 (C-N), 986 (C=C) cm^{-1}; elemental analysis calcd (%) for $C_{38}H_{68}N_4O_{12}Cl_4Ni_4\cdot 0.25\,Et_2O$: C 40.62, H 5.36, N 4.19; found: C 40.25, H 5.71, N 5.07.

$[Ni_4(HL1)_2(OMe)_2(MeOH)_2Cl_{2.8}F_{1.2}]\cdot Et_2O$ (C3). To a solution of H_2**L1** (0.100 g, 0.308 mmol) in MeOH (5 mL) was added solutions of $Ni(BF_4)_2\cdot 6H_2O$ (0.105 g, 0.308 mmol, 1 eq.) and $NiCl_2\cdot 6H_2O$ (0.0732 g, 0.308 mmol, 1 eq.), both in MeOH (7.5 mL). The green solution was stirred at RT for 10 minutes, followed by the addition of Et_3N (0.260 mL, 1.85 mmol, 6 eq.). The solution was stirred for a further 10 minutes at RT. Isolation of the complex was achieved by the diffusion of Et_2O into the reaction solution. Green platelet shaped X-ray quality crystals were produced after three weeks. The crystals were crushed and air dried prior to further analysis. Yield (0.070 g, 19%); IR: $\bar{\upsilon}$ = 3159 (O-H), 2947 (C-H), 1559 (C=N), 1463 (C=C), 1279 (O-H), 1218 (C-O), 1127 (C-O), 1020 (C-N) cm^{-1}; elemental analysis calcd. (%) for $C_{38}H_{68}N_4O_{12}Cl_{2.8}F_{1.2}Ni_4\cdot Et_2O$: C 41.90, H 6.53, N 4.65; found: C 41.80, H 6.64, N 4.44.

$[Ni_4(HL1)_2(OMe)_2(OAc)_2Cl_2]\cdot(MeOH)_2$ (C4) To a solution of H_2**L1** (0.200 g, 0.616 mmol, 1 eq.) in MeOH (20 mL) was added solutions of $Ni(OAc)_2\cdot 4H_2O$ (0.153 g, 0.616 mmol, 1 eq.) and $NiCl_2\cdot 6H_2O$ (0.146 g, 0.616 mmol, 1 eq.), both in MeOH (15 mL). The green solution was stirred at RT for 10 minutes, followed by the addition of Et_3N (0.520 mL, 3.70 mmol, 6 eq.). The solution was stirred for a further 10 minutes at RT. Isolation of the complex was achieved by the diffusion of Et_2O into the reaction solution. Green prism shaped X-ray quality crystals were produced after three weeks. The crystals were crushed and air dried prior to further analysis. Yield (0.140 g, 19%); IR: $\bar{\upsilon}$ = 3255 (O-H), 2944 (C-H), 1575 (C=N), 1487 (C=C), 1472 (CH_2), 1417 (N-O), 1331 (O-H), 1219 (C-O), 1131 (C-O), 1027 (C-N) 990 (C=C) cm^{-1}; elemental analysis calcd. (%) for $C_{40}H_{66}N_4O_{14}Cl_2Ni_4\cdot$MeOH: C 42.28, H 6.06, N 4.81; found: C 42.82, H 6.07, N 4.83.

Conflicts of interest

There are no conflicts to declare.

References

1 K. Griffiths, A. C. Tsipis, P. Kumar, O. P. Townrow, A. Abdul-Sada, G. R. Akien, A. Baldansuren, A. C. Spivey and G. E. Kostakis, *Inorg. Chem.*, 2017, **56**, 9563–9573.
2 F. Liu, F. Yang, H. Chen, Q. Chen, P. Yan and G. Li, *J. Inorg. Organomet. Polym. Mater.*, 2014, **24**, 259–266.
3 A. Das, M. Chakraborty, S. Maity and A. Ghosh, *Dalton Trans.*, 2019, **48**, 9342–9356.
4 Y. Wu, J. Y. Wang, L. Y. Zhang, L. J. Xu and Z. N. Chen, *Inorg. Chem.*, 2020.
5 K. Liu, W. Shi and P. Cheng, *Coord. Chem. Rev.*, 2015, **289**, 74–122.
6 C. J. Milios, A. Vinslava, W. Wernsdorfer, S. Moggach, S. Parsons, S. P. Perlepes, G. Christou and E. K. Brechin, *J. Am. Chem. Soc.*, 2007, **129**, 2754–2755.
7 C. I. Yang, K. H. Cheng, S. P. Hung, M. Nakano and H. L. Tsai, *Polyhedron*, 2011, **30**, 3272–3278.
8 Y. Peng, V. Mereacre, C. E. Anson and A. K. Powell, *Dalton Trans.*, 2017, **46**, 5337–5343.
9 Y. Peng and A. K. Powell, *Coord. Chem. Rev.*, 2021, **426**, 213490–213538.
10 S. K. Langley, N. F. Chilton, M. Massi, B. Moubaraki, K. J. Berry and K. S. Murray, *Dalton Trans.*, 2010, **39**, 7236–7249.
11 A. M. Ako, V. Mereacre, I. J. Hewitt, R. Clerac, L. Lecren, C. E. Anson and A. K. Powell, *J. Mater. Chem.*, 2006, **16**, 2579–2586.
12 C. P. Richers, J. A. Bertke, D. L. Gray and T. B. Rauchfuss, *Acta Crystallogr. E Crystallogr. Commun.*, 2015, **71**, 976–979.
13 G. Peng, G. E. Kostakis, Y. Lan and A. K. Powell, *Dalton Trans.*, 2013, **42**, 46–49.
14 K. Vignesh, S. Langley, K. Murray and G. Rajaraman, *Inorg. Chem.*, 2017, **56**, 2518–2532.
15 J. Rinck, Y. Lan, C. E. Anson and A. K. Powell, *Inorg. Chem.*, 2015, **54**, 3107–3117.

View Article Online
DOI: 10.1039/D0DT04286B

16 T. Han, W. Shi, Z. Niu, B. Na and P. Cheng, *Chem.*, 2013, **19**, 994–1001.
17 M. N. Akhtar, V. Mereacre, G. Novitchi, J. P. Tuchagues, C. E. Anson and A. K. Powell, *Chem.*, 2009, **15**, 7278–7282.
18 T. Glaser and T. Lugger, *Inorg. Chim. Acta*, 2002, **337**, 103–112.
19 C. Das, A. Upadhyay and M. Shanmugam, *Inorg. Chem.*, 2018, **57**, 9002–9011.
20 S. Demir, J. M. Zadrozny, M. Nippe and J. R. Long, *J. Am. Chem. Soc.*, 2012, **134**, 18546–18549.
21 L. Jiang, D. Y. Zhang, J. J. Suo, W. Gu, J. L. Tian, X. Liu and S. P. Yan, *Dalton Trans.*, 2016, **45**, 10233–10248.
22 I. Oyarzabal, J. Ruiz, A. J. Mota, A. Rodriguez-Dieguez, J. M. Seco and E. Colacio, *Dalton Trans.*, 2015, **44**, 6825–6838.
23 C. J. Milios, S. Piligkos and E. K. Brechin, *Dalton Trans.*, 2008, 1809–1817.
24 K. Mason, J. Chang, E. Garlatti, A. Prescimone, S. Yoshii, H. Nojiri, J. Schnack, P. A. Tasker, S. Caretta and E. K. Brechin, *Chem. Commun.*, 2011, **47**, 6018–6020.
25 R. Inglis, C. J. Milios, L. F. Jones, S. Piligkos and E. K. Brechin, *Chem. Commun.*, 2012, **48**, 181–190.
26 T. Yao, J. Lu, D. Li and J. Dou, *Acta Cryst.*, 2014, **C70**, 364–367.
27 A. S. Dinca, C. Maxim, B. Cojocaru, F. Lloret, M. Julve and M. Andruh, *Inorg. Chim. Acta*, 2016, **440**, 148–153.
28 C. J. Milios, A. Prescimone, A. Mishra, S. Parsond, W. Wernsdorfer, G. Christou, S. P. Perlepes and E. K. Brechin, *Chem. Commun.*, 2007, 153–155.
29 N. F. Chilton, R. P. Anderson, L. D. Turner, A. Soncini and K. S. Murray, *J. Comput. Chem.*, 2013, **34**, 1164–1175.
30 G. Rogez, J. Rebilly, A. L. Barra, L. Sorace, G. Blondin, N. Kirchner, M. Duran, J. van Slageren, S. Parsons, L. Ricard, A. Marvilliers and T. Mallah, *Angew. Chem.*, 2005, **117**, 1910–1913.
31 J. Titis and R. Boca, *Inorg. Chem.*, 2010, **49**, 3971–3973.
32 S. K. Singh, T. Gupta, P. Badkur and G. Rajaraman, *Chem. Eur. J.*, 2014, **20**, 10305–10313.
33 J. Titis, R. Boca, L. Dlhan, T. Durcekova, H. Fuess, R. Ivanikova, V. Mrazova, B. Papankova and I. Svoboda, *Polyhedron*, 2007, **26**, 1523–1530.
34 M. K. Singh and G. Rajaraman, *Inorg. Chem.*, 2019, **58**, 3175–3188.
35 M. A. Halcrow, J. S. Sun, J. C. Huffman and G. Christou, *Inorg. Chem.*, 1995, **34**, 4167–4177.
36 K. K. Nanda, L. K. Thompson, J. N. Bridson and K. Nag, *J. Chem. Soc., Chem. Commun.*, 1994, 1337–1338.
37 L. Ballester, E. Coronado, A. Gutierrez, A. Monge, M. F. Perpinan, E. Pinilla and T. Rico, *Inorg. Chem.*, 1992, **31**, 2053–2056.
38 S. Hazra, S. Bhattacharya, M. K. Singh, L. Carella, E. Rentschler, T. Weyhermueller, G. Rajaraman and S. Mohanta, *Inorg. Chem.*, 2013, **52**, 12881–12892.
39 M. K. Singh and G. Rajaraman, *Chem. Eur. J.*, 2015, **21**, 980–983.
40 J. Cano, E. Ruiz, S. Alvarez and M. Verdaguer, *Comments, Inorg. Chem.*, 1998, **20**, 27–56.
41 R. Aldred, R. Johnston, D. Levin and J. Neilan, *J. Chem. Soc., Perkin Trans. 1*, 1994, **13**, 1823–1831.
42 P. Meier, F. Broghammer, K. Latendorf, G. Rauhut and R. Peters, *Mol.*, 2012, **17**, 7121–7150.
43 *Crystal Clear*, Rigaku Americas Corporation, The Woodlands, Texas, 1st edn, 2005.
44 *PROCESS-AUTO*, Rigaku Corporation, Tokyo, 1st edn, 1998.
45 O. V. Dolomanov, L. J. Bourhis, R. J. Gildea, J. A. K. Howard and H. Puschmann, *J. Appl. Cryst.*, 2009, **42**, 339–341.
46 L. Palatinus, S. J. Prathapa and S. van Smaalen, *J. Appl. Cryst.*, 2012, **45**, 575–580.
47 L. Palatinus and A. van der Lee, *J. Appl. Cryst.*, 2008, **48**, 975–984.
48 L. Palatinus and G. Chapuis, *J. Appl. Cryst.*, 2007, **40**, 786–790.
49 G. M. Sheldrick, *Acta Crystallogr. C. Struct. Chem.*, 2015, **71**, 3–8.
50 M. J. Frisch, G. W. Trucks, H. B. Schlegel, G. E. Scuseria, M. A. Robb, J. R. Cheeseman, G. Scalmani, V. Barone, G. A. Petersson, H. Nakatsuji, X. Li, M. Caricato, A. V. Marenich, J. Bloino, B. G. Janesko, R. Gomperts, B. Mennucci, H. P. Hratchian, J. V. Ortiz, A. F. Izmaylov, J. L. Sonnenberg, D. Williams-Young, F. Ding, F. Lipparini, F. Egidi, J. Goings, B. Peng, A. Petrone, T. Henderson, D. Ranasinghe, V. G. Zakrzewski, J. Gao, N. Rega, G. Zheng, W. Liang, M. Hada, M. Ehara, K. Toyota, R. Fukuda, J. Hasegawa, M. Ishida, T. Nakajima, Y. Honda, O. Kitao, H. Nakai, T. Vreven, K. Throssell, J. A. Montgomery, Jr., J. E. Peralta, F. Ogliaro, M. J. Bearpark, J. J. Heyd, E. N. Brothers, K. N. Kudin, V. N. Staroverov, T. A. Keith, R. Kobayashi, J. Normand, K. Raghavachari, A. P. Rendell, J. C. Burant, S. S. Iyengar, J. Tomasi, M. Cossi, J. M. Millam, M. Klene, C. Adamo, R. Cammi, J. W. Ochterski, R. L. Martin, K. Morokuma, O. Farkas, J. B. Foresman and D. J. Fox, *Gaussian~16 Revision C.01*, 2016, Gaussian Inc. Wallingford CT.
51 C. Lee, W. Yang and R. G. Parr, *Phys. Rev. B*, 1988, **37**, 785.
52 A. D. Becke, *J. Chem. Phys.*, 1993, **98**, 5648.
53 A. D. Becke, *J. Chem. Phys.*, 1993, **98**, 1372–1377.
54 P. J. Stephens, F. J. Devlin, C. F. Chabalowski and M. J. Frisch, *J. Chem. Phys.*, 1994, **98**, 11623–11627.
55 A. Schafer, H. Horn and R. Ahlrichs, *J. Chem. Phys.*, 1992, **97**, 2571.
56 A. Schafer, C. Huber and R. Ahlrichs, *J. Chem. Phys.*, 1994, **100**, 5829.
57 G. E. Scuseria and H. F. Schaefer, *J. Chem. Phys.*, 1989, **90**, 3700–3703.
58 P. C. Hariharan and J. A. Pople, *Theoret. Chim. Acta (Berl.)*, 1973, **28**, 213–222.
59 L. Noodleman and J. G. Norman, *J. Chem. Phys.*, 1979, **70**, 4903.
60 L. Noodleman, *J. Chem. Phys.*, 1981, **74**, 5737.
61 L. Noodleman and E. R. Davidson, *Chem. Phys.*, 1986, **109**,

View Article Online
DOI: 10.1039/D0DT04286B

131–143.
62 L. Noodleman and D. A. Case, *Adv. Inorg. Chem.*, 1992, **38**, 423–470.
63 J. H. Van Vleck, *The theory of electric and magnetic susceptibilities*, Oxford University Press, 1930.
64 J. J. Borras-Almenar, J. M. Clemente-Juan, E. Coronado and B. S. Tsukerblat, *J. Comput. Chem.*, 2001, **22**, 985–991.